Multiplane scanning Stereo-PIV measurements of flow inside a spiral vortex pulsatile blood pump

Takanobu Yagi[1,2], William Yang[2], Daisuke Ishikawa[1], Hiroyuki Sudo[1], Kiyotaka Iwasaki[3], Mitsuo Umezu[1]

1: Integrative Bioscience and Biomedical Engineering, Waseda University, Tokyo, Japan,
takanobu_yagi@akane.waseda.jp
2: Division of Minerals, CSIRO, Melbourne, Australia,
william.yang@csiro.au
3: Institute for Biomedical Engineering, Waseda University, Tokyo, Japan,
iwasaki@waseda.jp

Abstract A multiplane scanning Stereo-PIV (MS-SPIV) system was developed to allow three-dimensional volume mapping measurements of Stereo PIV in liquid flows enclosed by complex geometries, such as biomedical flows. The optical system was constructed on a motorized scanning stage. After a single-plane in-situ 3D calibration, refractive-index matched dynamic prisms enabled to traverse Stereo-PIV measurements in out-of-plane directions regardless of the complex model geometries. MS-SPIV measurements were carried out inside a spiral vortex (SV) pulsatile blood pump. The present study aims to reveal the mechanism of the highly three-dimensional unsteady vortex. A full-scale Perspex model of the SV pump was used in an in vitro cardiovascular flow simulator. Typical driving conditions were adopted as follows: a heart rate of 72 beats/min, averaged flow rate of 5.0 L/min and systolic fraction of 32%. The mean bulk Reynolds number Re_{mean} and the Womersley number Wo were approximately Re_{mean} = 1600 and Wo=15, respectively. Phase-locked MS-SPIV measurements enabled to reveal the complex behaviour of the three-dimensional unsteady vortex. The results demonstrated that an initial vortex structure developed during filling was a principal factor of determining a near-wall swirling velocity gradient during systole. Although the diastolic vortex was expected to have an axisymmetric vortex structure so as to produce a uniform wall shear rate throughout a diaphragm-housing junction, it was found that the rotating axis was inclined with respect to the pump centerline. Among several relevant factors, it was demonstrated that the filling flow inside a chamber exhibited a significant diffusivity towards a pump apex.

1. Introduction

Thromboembolism is one of the major morbidity events in clinical applications of pulsatile artificial hearts (Deng et al., 2005). It is generally believed that flow physics has a deep relationship with thrombus formation. Thus, there are a large number of experimental studies relating to the flow inside a pulsatile artificial blood pump. Jin and Clark (1993) made LDA measurements within a pneumatically-driven artificial blood pump. They presented a 'washing' flow by a main vortex developed during filling, and revealed local flow recirculation as an underlying risk of thrombus formation. The similar vortex formations were observed in accordance with pump geometries by several researchers (Betram and Nugent, 1993, Akutsu et al., 1999, Mussivand et al., 1999). In a group of Pennsylvania State University, fluid mechanics of a pulsatile artificial heart has been extensively studied. Baldwin et al. (1993, 1994) reported mean velocity and Reynolds stress fields within the Penn State pulsatile artificial heart using LDA. They observed no flow stagnation persistent through a cardiac cycle. In later years, Hochareon et al. (2004) reported phase-locked 2D velocity and vorticity fields of a main vortex within their smaller-scaled 50cc blood pump using 2D-PIV. Deutsch et al. (2006) reviewed their historical achievements of the Penn State pulsatile artificial heart.

Although a majority of those documented experimental investigations provided a certain design rationale of a pulsatile artificial blood pump, the design criteria are still obscure owing to the complex flow. The flow inside a pulsatile artificial blood pump behaves as a highly three-dimensional (3D) unsteady vortex. The vortex is initiated by tangential filling flow while it is highly skewed by an inflow jet through an inlet valve. This initial vortex, during systole, is ejected by a large deformation of a membrane while it is again distorted by an outflow jet through an outlet valve. This complex flow makes it unattainable to understand the structure using conventional flow diagnostic systems such as LDA and 2D-PIV. As a result, the structure of three-dimensional vortex has never been discussed, although fluid mechanics of a pulsatile blood pump is essentially to control the unsteady behaviour. Our first scope is, thus, to visualize the structure of three-dimensional unsteady vortex in a quantitative manner.

The present paper describes a novel multiplane scanning Stereo-PIV (MS-SPIV) system that has been developed in our group in order to allow three-dimensional volume mapping measurements of Stereo PIV in liquid flows enclosed by complex geometries. Such confined complex flows are often seen in biomedical applications such as artificial organs and blood vessels. MS-SPIV was motivated from high demands for three-dimensional quantitative flow visualization in biofluid mechanics. MS-SPIV was applied to the flow inside a spiral vortex pulsatile blood pump. The present study aims to demonstrate the unsteady behaviour of three-dimensional vortex and to reveal principal factors of determining the three-dimensional structure with an emphasis on the near-wall flow fields.

2. Methods

2.1 Spiral vortex pulsatile blood pump

A spiral vortex pulsatile blood pump (hereinafter refer to as SV pump) is an inexpensive first-aid-type pneumatically-driven ventricular assist device. The detailed descriptions are documented elsewhere (Iwasaki et al., 2002; Nugent et al., 1991; Sudo et al., 2005; Umezu et al., 1991). We therefore briefly describe the overview. Fig.1 presents the side and overhead views. The SV pump consists of three parts: housing, diaphragm and base. The basic material is a sheet of polyurethane. Their shapes are vacuum-formed individually and assembled by high-frequency welding. The blood chamber is conical-shaped, which has an inflow conduit angled 35 deg downward in the tangential direction and an outflow conduit at the apex. Polymeric heart valves are installed in both conduits to yield unidirectional flows. This unique design aims to reduce the risk of thrombus formation by producing a continuous swirling flow throughout a cardiac cycle. A diaphragm-housing junction is historically recognized as one of the frequent sites of thrombus formation. Since the nearby flow may have a more likelihood of stagnation, which yields a favorable situation for thrombus formation, the SV pump is expected to direct a ‘washing’ flow into the diaphragm-housing junction by tangential inflow.

2.2 Pulsatile flow rig

A full-scale Perspex model of the SV pump was used in the present study. A Perspex block was machined to form a housing inside and a flat surface outside. The pump base was machined in the same way and assembled with a diaphragm. The polyurethane diaphragm is a concave-shaped membrane of 0.6 mm thickness. Fig.2-3 presents a pulsatile flow rig and typical pressure and flow-rate waveforms. The pressures were measured using a conduit-type pressure transducer in the height of the diaphragm-housing junction. The Perspex SV pump was driven by a pneumatic pressure driver. An external pulsation unit controls the pressure timing. The pulsatile-flow rig consists of a preload tank and an afterload circuit to simulate physiological cardiovascular waveforms. A Newtonian blood-analog refractive-index-matched liquid was used as a working fluid. The fluid

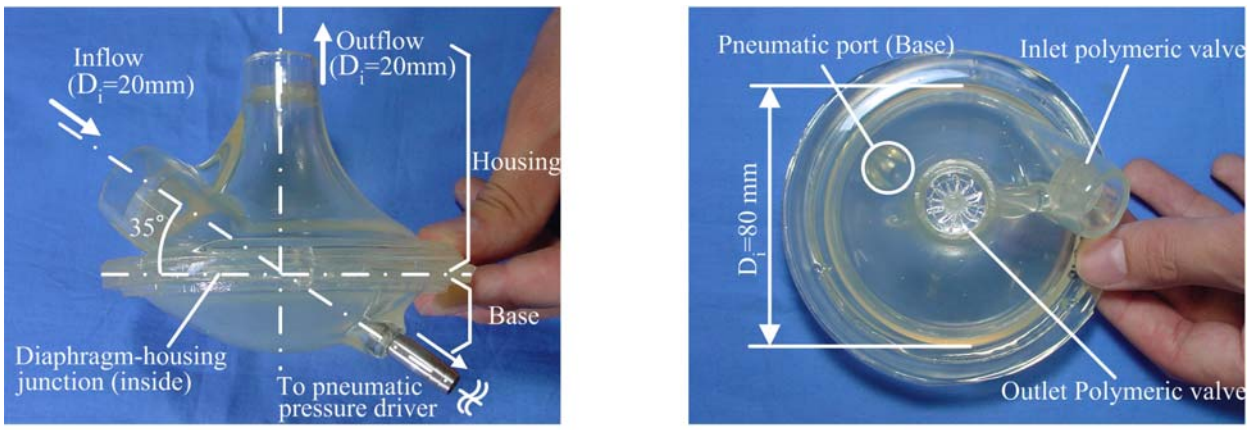

(a) Side view (b) Overhead view

Fig.1 Spiral vortex pulsatile blood pump (D_i: internal diameter)

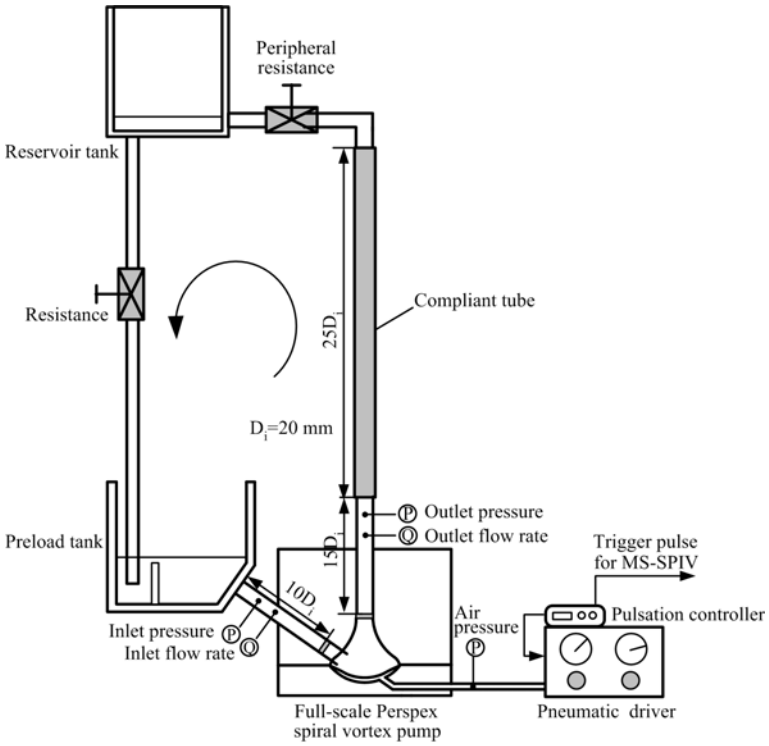

Fig.2 Pulsatile flow rig

consisted of a mixture of saturated aqueous sodium iodide, glycerol and distilled water, 79/20/1 by volume, respectively. The density and kinematic viscosity was ρ= 1700 Kg/m^3, ν= 3.3 cSt, respectively. The refractive index was adjusted at 1.492 at room temperature under the 532-nm wavelength using a multiple-wavelength Abbe refractometer (DR-M2, ATAGO Co., Ltd., Tokyo). Typical driving conditions were adopted as a bench-mark test as follows: a heart rate of 72 beats/min, mean flow rate of 5.0 L/min and systolic fraction of 32%. The mean bulk Reynolds number Re_{mean} and the Womersley number *Wo* were approximately Re_{mean} = 1600 and *Wo*=15 based on the diameter of inlet and outlet conduit (20 mm).

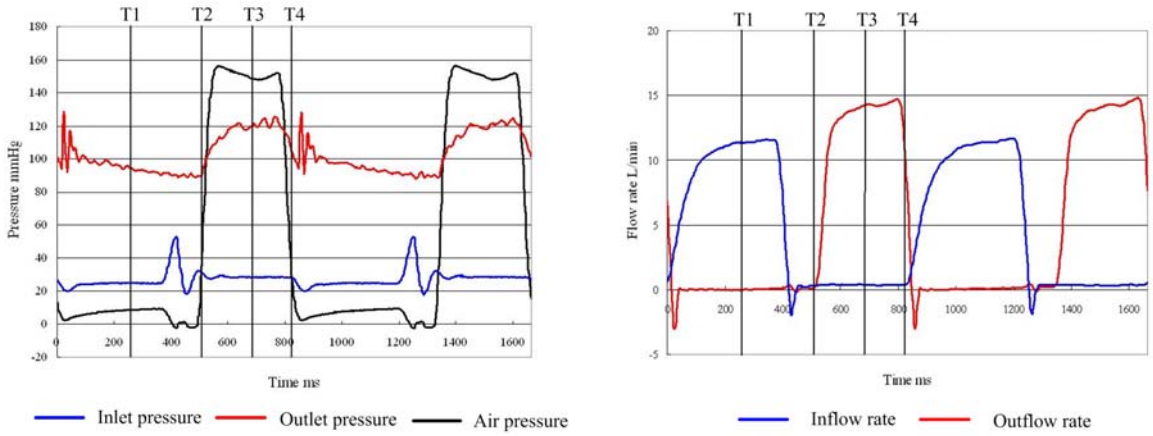

Fig.3 Pulsatile flow waveforms (left: pressure, right: flow rate) in a cardiovascular flow simulator. T1-4 shows time phases for phase-locked measurements (T1: t/T=0.31, Mid diastole, T2: t/T=0.62, Sytole onset, T3: t/T=0.84, Mid systole, T4: t/T=0.99, End systole, T: cardiac cycle)

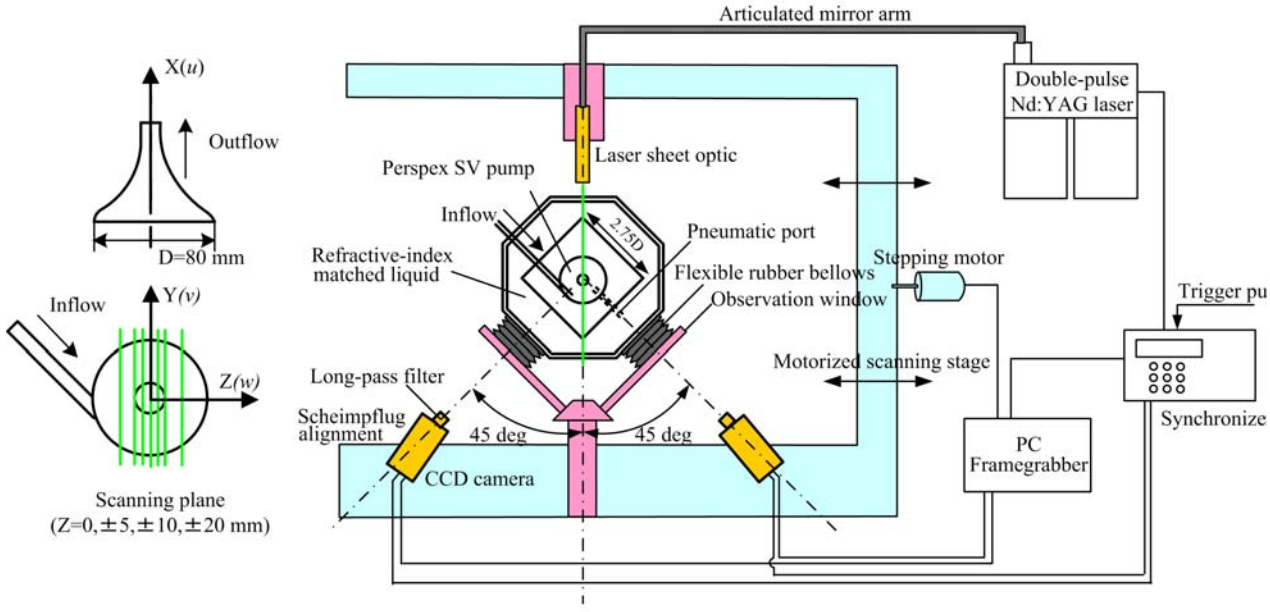

Fig.4 Overhead view of MS-SPIV setup. Scanning planes were illustrated in the left side

2.3 Multiplane scanning Stereo PIV

Prior to the present study, the measurement accuracy of SPIV was studied in a steady spiral flow inside the same Perspex SV pump by comparing the mean velocity results with those measured by LDA and 2D-PIV (Yagi et al., 2005). Those results yielded design guidelines of MS-SPIV. Fig.4 illustrates the overhead view. As previously mentioned, MS-SPIV was specifically designed to allow three-dimensional volume mapping of Stereo PIV in liquid flows enclosed by complex geometries. A 45-degree back-scattered Scheimpflug Stereo-PIV alignment was adopted. In order to allow the scanning measurement, the optical system was constructed on a motorized scanning stage. Both dual cameras and a laser light sheet optic were simultaneously traversed in the out-of-plane direction using a stepping motor. In order to ensure an identical mapping function in any scanning position, a *dynamic prism* was developed. It consisted of an octagonal Perspex tank

installed with dual flexible rubber bellows and Perspex observation windows. This mechanism was filled entirely with the same refractive-index matched liquid as a working fluid, and installed into the motorized scanning stage. Thus, the initial optical alignment is not altered in any scanning position owing to the flexible bellows. The observation windows are passively positioned by the stepping motor with respect to measurement planes. The advantage of this system setup only requires a single in-situ calibration, and afterwards Stereo-PIV measurements are repeated in any position of interest. This method ideally cancels out the multiple curvatures of complex model geometries and allows three-dimensional volume mapping of Stereo-PIV measurements in liquids.

The optical hardware consisted of two 12-bit CCD cameras (1280×1024 pixels, PCO SensiCam, PCO, Germany) and a two-cavity double-pulse Nd:YAG laser (Solo PIV, New Wave Research, Inc., CA, U.S.A.) of nominal 120 mJ. A commercial PIV software (VidPIV 4.6, Intelligent Laser Application Gmbh, Germany) was used for software processing. The scanning positions were set at seven z-planes as illustrated in Fig.4. Phase-locked measurements were made in mid diastole, systole onset, mid systole and end systole as shown in Fig.3. The velocity vectors were averaged through 600 pulsatile cycles.

In-situ 3D calibrations (Soloff et al., 1997) were carried out without the Perspex SV pump where the identical optical conditions were reproduced with the same refractive-index matched liquid. A calibration target consisted of multiple dot marks printed in a transparency sheet, which was clamped by Perspex plates. The calibration plate was translated in a normal direction of the laser light sheet by a manual linear stage with a precision micrometer (UMR 8.51, BM 17.51, Newport Corporation, CA, U.S.A). A set of calibration images were recorded at 5 different depths inside the laser light sheet of approximately 2.5-mm thickness. The mapping function was defined to be cubic in an in-plane direction and quadratic in an out-of-plane direction. In order to minimize the uncertainty of defining the center of dot marks, a pattern-matching method was used. In PIV processing, a multi-pass cross correlation scheme was used. The final interrogation region was 32×32 pixels (2.0×2.0 mm^2) with 50 % overlap.

Seeding particles used were novel fluorescent particles (D=18 μm, ρ=1500 Kg/m^3) that has been developed under a collaborative project with Sekisui Plastics Co., Ltd., Japan. There are high demands for measuring wall shear rates in biofluid mechanics. Although MS-SPIV is expected to yield entire wall-shear-rate distributions in artificial organs and blood vessels, this parameter estimation is not straightforward. Owing to a distinct refractive-index material such as a diaphragm and a heart valve, the wall light reflections had to be minimized carefully to allow near-wall measurements as accurately as possibly. The novel fluorescent particles have been specifically designed for PIV measurements and optimized with relevant parameters to enhance the image visibility. As shown in Fig. 4, long-pass optical filters were installed into both cameras to cut off reflections and pass fluorescent emission lights.

3. Results and discussion

3.1 Unsteady vortex behaviour

We first describe the unsteady behaviour of the vortex based on a phase-locked analysis through a cardiac cycle. Fig.5-9 summarizes the results of four different time phases (Fig.3) at the center plane (Z=0 mm, ref. Fig.4). Fig.5-6 shows tangential and axial velocity profiles at selective points at X=5, 15, 25, 35 mm (ref. Fig.7-9). The velocity plots of X=5 mm at end systole was blocked by a diaphragm. Wall boundaries are showed by dot lines. Fig.7 presents the contour plots of tangential velocity. Fig.8 shows an in-plane velocity (u, v) vector plots, and Fig.9 shows the contour plots of the axial velocity. In SPIV processing, the masking of wall boundaries was not included due to the

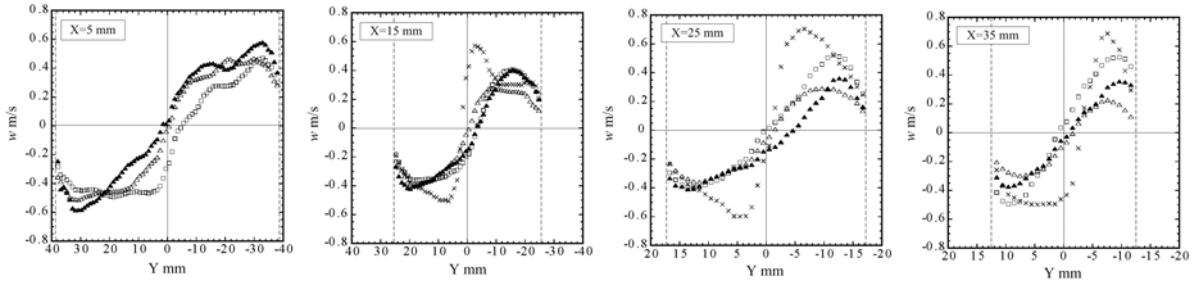

Fig.5 Phase-locked mean tangential velocity plots at X=5, 15, 25 and 35 mm
(t/T=0.31(△), 0.62(▲), 0.84(□), 0.99(×)). Wall boundaries are shown with dot lines

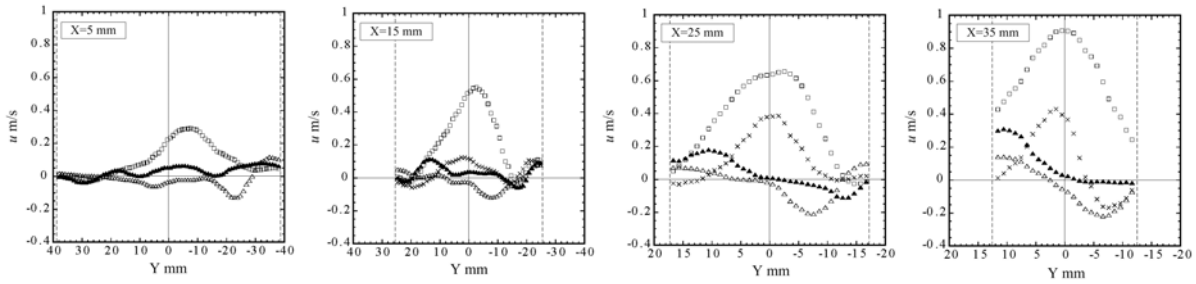

Fig.6 Phase-locked mean axial velocity plots at X=5, 15, 25 and 35 mm
(t/T=0.31(△), 0.62(▲), 0.84(□), 0.99(×)). Wall boundaries are shown with dot lines

ambiguity of image boundaries. After three-component velocity reconstructions, wall boundaries were strictly defined based on the real pump design except a diaphragm, and the vectors seen outside the pump are chopped off. An outlet valve was located immediately downstream of the top edge of those field plots.

As shown in Fig.5, the swirling motion was structurally changed towards end systole. From mid diastole to mid systole, free-vortex-type motions were dominant. At end systole, the core vortex became a forced-vortex-type motion of a steep velocity gradient. This end-systole vortex was similar to the vortex in a steady flow as previously investigated (Yagi et al., 2005). Thus, this structural change was expected to be induced by an outflow. The outward swirling motion inside the conical housing worked favourably to increase the swirling velocity in consideration of the angular momentum. This was more remarkably observed in the core region than in the wall region owing to the tangential wall friction. This yielded a relatively stable near-wall tangential velocity, especially in the lower region of the housing. The velocity of approximately 0.2 m/s was not varied significantly throughout a cardiac phase. Towards an apex, the core vortex became dominant over the cross-sectional plane. Thus, the larger variations of the near-wall tangential velocity, which ranged between approximately 0.2 to 0.5 m/s, were observed at X=35 mm. In the axial motion, similar observances were demonstrated. Towards the apex, the near-wall axial velocity gradient exhibited greater temporal variations owing to a nozzle effect. It was believed that the wall shear rate may exhibit a greater temporal variation towards the apex. Although the shear rate mapping did not lie in the present scope, this knowledge is quite useful towards the achievement.

The unsteady behaviour of the swirling motion is further studied using Fig.7. At mid diastole, the main swirl was observed near the diaphragm-housing (DH) junction. This is expected to work favourably to reduce the risk of thrombus formation at the DH junction. The contour plots showed that the tangential velocity was distributed in an asymmetric manner. In the positive Y-axis (viz. circumferentially farther from the inlet side), the distribution became more broadened towards the apex. In consideration of the downward inflow (ref. Fig.1), this phenomenon implied that the

swirling streamlines were diffusive as it travelled along the housing circumferentially. This is further studied later three-dimensionally. At the onset of systole, the similar swirl was observed, although the filling into the chamber was already ended before the onset as shown by a sudden rise of inlet pressure in Fig.3. This revealed that the swirling motion was continuously formed along the DH junction regardless of the inlet valve closure. This swirling motion, as the diaphragm started to move upward, was shifted upward as well as outward. This shifting flow produced further tangential velocity gradient near the wall. As the diaphragm appeared in the field-of-view at mid systole, the main swirl was further shifted towards the apex. From this finding, it can be said that the near-wall swirl motion was shifted quite sensitively towards the apex in accordance with the diaphragm motion. This is a favourable result in terms of 'washing' inside the blood chamber. Meanwhile, the swirling motion on the top of the diaphragm was highly complex and asymmetric. It was observed that the diaphragm behaved in an asymmetric manner towards the top position. Several relevant factors are responsible for the behaviour, such as a nonaxisymmetric structure of a mid-diastolic vortex (discussed later), a pneumatic port inside the base and a buckling of the diaphragm. Further experiments will be required to reveal the flow structure on the top side of a moving diaphragm. During systole, the core of the swirling motion was significantly skewed by the upward-moving diaphragm. This implies that the vortex was highly asymmetric and single-plane investigations may not be applied into the three-dimensional space. This is emphasized further in the later discussion.

Unsteady axial motions are studied using Fig.8-9. Phase-locked axial motions explained highly three-dimensional complex behaviour of the global vortex. At mid diastole, three characteristic motions were detected: downward inflow, near-wall rising swirl and large recirculation. The rising swirl was found in the immediate upside of the downward inflow. This flow mechanism was not clarified with the single-plane investigation, and explained later with an aid of MS-SPIV. The large recirculation was induced by the bouncing flow at the outlet valve. In consideration of the swirling velocity, this implies that the rotating axis of the global vortex was inclined with respect to the pump centreline, and this is further verified later. At the onset of systole when the outlet valve was in the beginning stage of opening, similar, but clearer upward motions were observed. Interestingly, it was demonstrated that the nonaxisymmetric vortex structure at mid diastole has strong effects on the initial development of the axial motion at early systole. The downward swirl at mid diastole worked like a damping factor and skewed the upward axial motion at the onset of systole. Meanwhile, the remaining downward inertia impinged the rising near-wall swirl. This implied that the rising swirl should have a continuous inertial supply in the out-of-plane direction in consideration of the relatively weak, but persistent upward velocity. At mid systole, the core flow was directed towards the outlet valve and showed the peak velocity of approximately 0.9 m/s. The similar, but more skewed motions were observed at end systole. During systole, the flow in an annular region was not clearly directed into the outlet valve, and highly anisotropic flows were observed. In terms of the residence time of blood remaining inside the chamber, the unsteady mechanism of the axial motion should be further investigated, especially during accelerating period.

As a summary of the unsteady behaviour, highly asymmetric flows observed throughout the cardiac cycle emphasized the necessity of the multiplane investigations. In consideration of the unsteady mechanism of the global vortex, the initial structure, namely the one at mid diastole, constitutes principal factors of determining the near-wall swirl structure during systole. If the diastolic flow structure is three-dimensionally axisymmetric, the upward swirl shifted by the moving diaphragm may work to reduce the risk of thrombus formation inside the entire chamber. This three-dimensionality of the initial vortex is studied next with an aid of MS-SPIV.

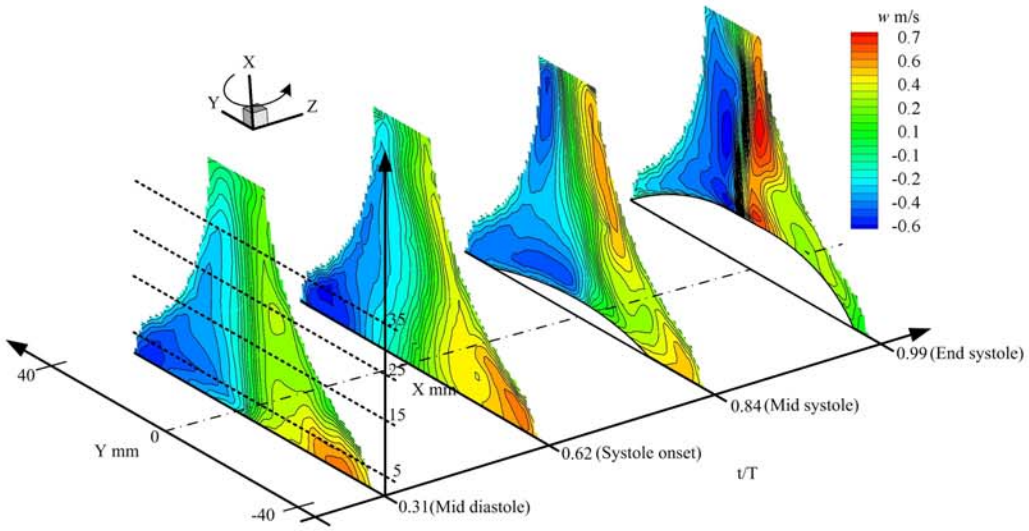

Fig.7 Phase-locked mean tangential velocity (w) distributions in a center plane (z=0 mm) measured by MS-SPIV

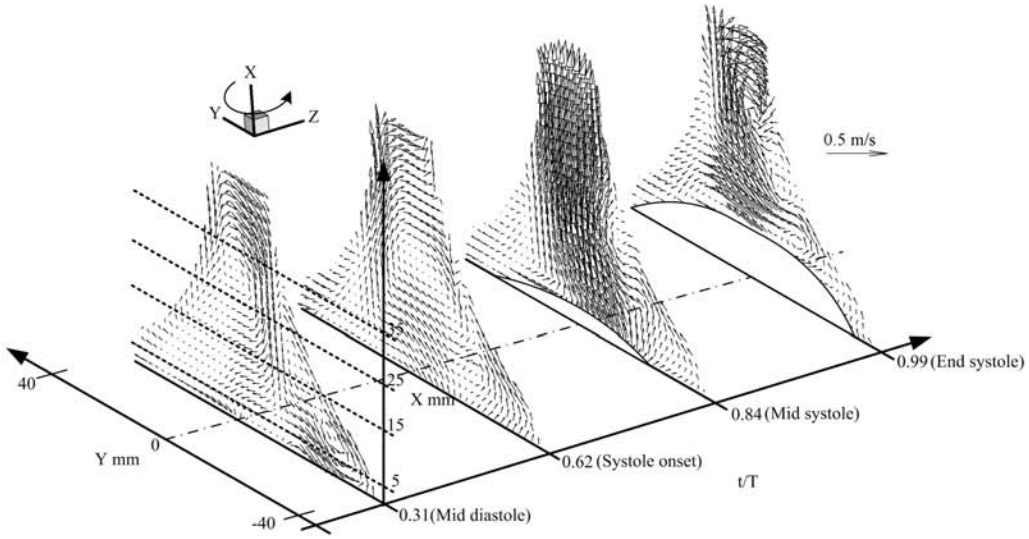

Fig.8 Phase-locked in-plane velocity vectors (u,v) in a center plane (z=0 mm) measured by MS-SPIV. Vectors were omitted by half for clarity.

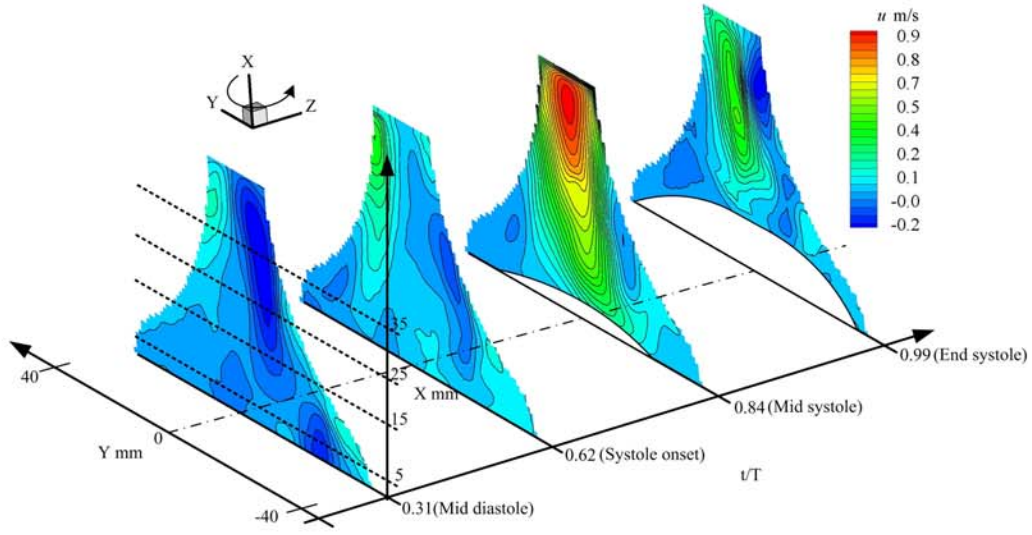

Fig.9 Phase-locked mean axial velocity (u) distributions in a center plane (z=0 mm) measured by MS-SPIV

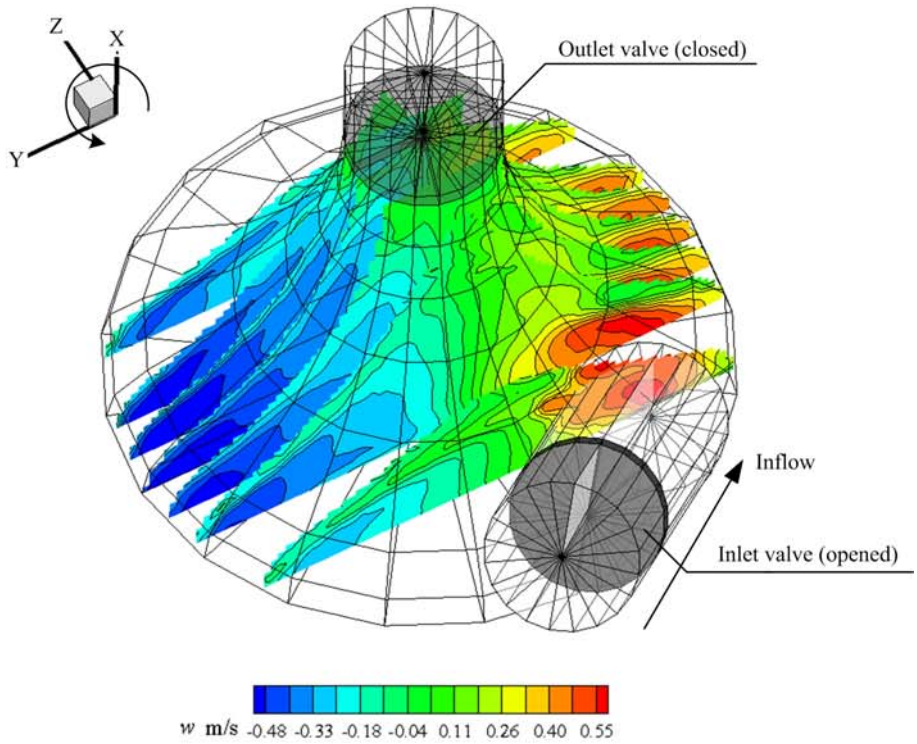

Fig.10 Mid-diastolic mean tangential velocity distributions using MS-SPIV

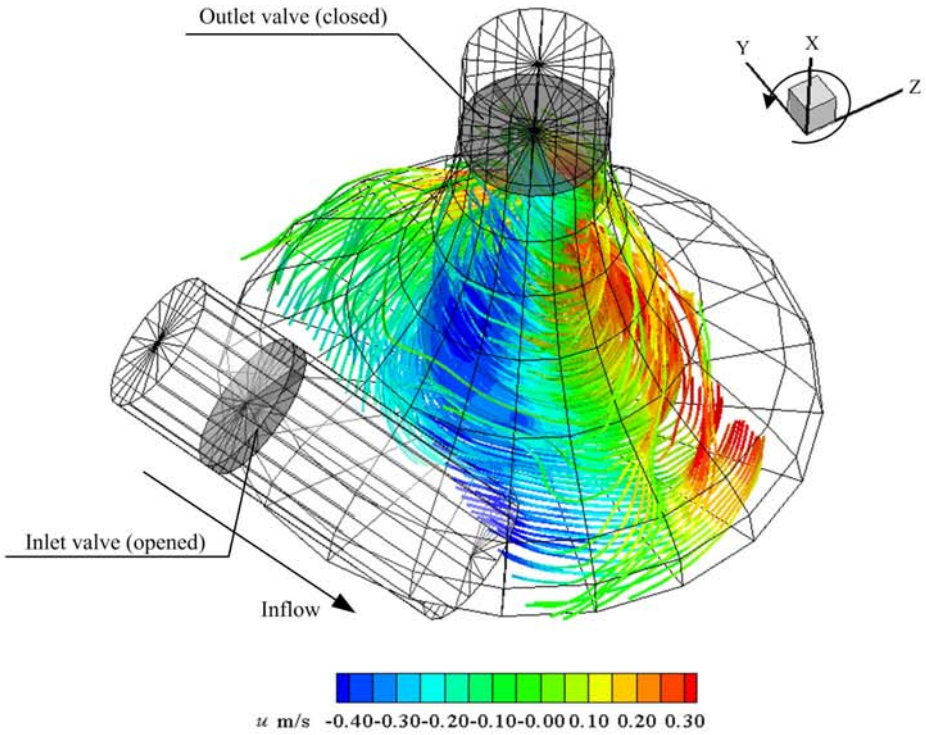

Fig.11 Mid-diastolic three-dimensional volumetric streamlines using MS-SPIV.
Color contour presents axial velocity.

3.2 Three-dimensional structure of mid-diastolic vortex

Fig.10-11 presents the three-dimensional vortex structure at mid diastole as measured by MS-SPIV. Fig.10 shows the mean tangential velocity distributions. Fig.11 presents the three-dimensional streamlines with the contour of axial velocity, which were reconstructed with three-component velocity vectors at 7 scanning planes. A pump chamber was drawn with a full-scale internal geometry together with the exact positions of inlet and outlet valves. Those valves were simply drawn with the disk shapes. The inlet conduit was simplified with a straight pipe.

As shown in Fig.10, strong swirling velocities were observed along the DH junction. In the immediate upside of the inlet downstream, the swirl was detached from the wall region, where the weak swirling velocity was observed. Although this region transiently experiences weak wall shear rate at mid diastole, the strong swirl observed in the downside may yield a 'washing' flow in early systole as shown previously. As the swirl travels along the conical housing, the spatial distributions of tangential velocity became more broadened at the circumferentially farther regions from the inlet conduit. Thus, the three-dimensional swirling structure was not axisymmetric with respect to the pump centreline. In the farthest region, the tangential velocity gradient became obscure. In consideration of the unsteady swirling behaviour, this region may persistently experience low wall shear rate throughout a cardiac cycle. Further investigations will be conducted to quantify the extent of weak tangential velocity gradients.

In Fig.11, the three-dimensional streamlines are studied for revealing principal factors of inducing the nonaxisymmetric vortex structure. From a fluid-mechanical point of view, it is essential to control this initial vortex structure so as to yield a sufficient wall shear rate throughout the DH junction during diastole and thereby throughout an entire pump chamber during systole. The nonaxisymmetric vortex structure was clearly demonstrated by the contour of axial velocity distributions. The rotating axis of the swirl was inclined with respect to the pump centreline. This skewed structure yielded a clearance gap in the wall region at the immediate upside of the inlet downstream, where a weak near-wall rising swirl was detected. In the further downstream, the main streamlines were abruptly directed towards the apex, and then bounced by the outlet valve to yield a downward swirling motion. Several relevant factors are expected to induce this inclined vortex structure, such as the orientation of the inlet conduit and the pneumatic port. Among them, it is believed that the filling flow inside a chamber, unlike a continuous expanding flow, exhibits the characteristics of greater diffusivity. As the tangential inflow filled the chamber, the main momentum inertia became significantly diffused upward in the direction of the outlet valve. This resulted in an obscure tangential velocity gradient observed in the circumferentially farthest region from the inlet conduit. Therefore, fluid mechanism of a pulsatile artificial blood pump may be essentially to control this diffusive tangential inflow.

4. Conclusion

In the present study, a novel multiplane scanning Stereo-PIV system was developed and applied to the highly three-dimensional unsteady vortex in a phase-locked manner inside a spiral vortex pulsatile blood pump. The unsteady vortex behaviour was clearly demonstrated, and revealed that the initial vortex structure developed during filling has the critical factor of determining near-wall swirling velocity gradients during systole. Although the diastolic vortex is expected to behave in an axisymmetric manner so as to produce a sufficient 'washing' flow throughout the diaphragm-housing junction, the rotating axis was inclined with respect to the pump centreline. Among several relevant factors, it was suggested that the filling flow inside a chamber behaved in a more diffusive manner than the continuous expanding flow inside the channel. This diffusive filling flow

constituted one of the principal factors of determining near-wall swirling velocity gradients from diastole to systole continuously.

In the perspective of the multiplane scanning Stereo-PIV system, the error analysis will be carried out with an aid of Laser Doppler Anemometry. Future topics will include turbulence and wall-shear-rate distributions throughout an entire pump chamber inside a pulsatile artificial heart. In the future, The MS-SPIV system will be also used to study three-dimensional unsteady flow in cardiovascular and cerebrovascular fields.

Acknowledgement

This research was organized by Biomedical Engineering Research on Advanced Medical Treatment, Advanced Research Institute for Science and Engineering, Waseda University (05P29), and it was financially supported by the 21st COE program of Waseda University (The innovative research on symbiosis technologies for human and robots in the elderly dominated society) and Health Science Research Grants (H17-F-003). This work was conducted under a collaborative project with CSIRO Minerals, Australia and the authors with to thank gratefully CSIRO Minerals for their valuable supports.

References

Akutsu T, Kase Y (1999) In vitro LDA and flow visualization analysis of the spiral vortex pump: effect of inlet valve orientation. Journal of Artificial Organs 2: 146-151

Baldwin JT, Deutsch S, Petrie HJ, Tarbell JM (1993) Determination of principal Reynolds stresses in pulsatile flows after elliptical filtering of discrete velocity measurements. Journal of Biomechanical Engineering 115: 396-403

Baldwin JT, Deutsch S, Geselowitz DB, Tarbell JM (1994) LDA measurements of mean velocity and Reynolds stress fields within an artificial heart ventricle. Journal of Biomechanical Engineering 116: 190-200

Betram CD, Nugent AH (1993) Flow visualization and measurement in a cardiac assist device. SPIE Laser Anemometry Advances and Applications 2052: 203-209

Deng MC, Edwards LB, Hertz MI et al. (2005) Mechanical circulatory support device database of the international society for heart and lung transplantation: Third annual report-2005. Journal of Heart and Lung Transplantation 24: 1182-1187

Deutsch S, Tarbell JM, Manning KB, Rosenberg G, Fontain AA (2006) Experimental fluid mechanics of pulsatile artificial blood pumps. Annual Review of Fluid Mechanics 38: 65-86

Hochareon P, Manning KB, Fontaine AA, Tarbell JM, Deutsch S (2004) Fluid dynamic analysis of the 50cc Penn State artificial heart under physiological operating conditions using particle image velocimetry. Journal of Biomechanical Engineering 126: 585-593

Iwasaki K, Umezu M, Tsujimoto T, Yoshida K, Saeki W, Qian Y, Ishihara K, Imachi K, Sakurai Y (2002) An inexpensive pulsatile blood pump: fabrication strategies and in vitro reliable methodology to evaluate blood compatibility. In Proceedings of the 11th International conference on Biomedical Engineering, Singapore

Jin W, Clark C (1993) Experimental investigation of unsteady flow behaviour within a sac-type ventricular assist device (VAD). Journal of Biomechanics 26(6): 697-707

Mussivand T, Day KD, Naber BC (1999) Fluid dynamics optimization of a ventricular assist device using particle image velocimetry. ASAIO Journal 45: 25-31

Nugent AH, Ye C-X, Umezu M, Chang VP (1991) In vitro visualization of the flow patterns of spiral vortex pump and a conventional ventricular assist device. Artificial Organs 14(4): 42-44

Soloff SM, Adrian RJ, Liu ZC (1997) Distortion compensation for generalized stereoscopic particle image velocimetry. Measurement Science and Technology 8: 1441-1454

Sudo T, Iwasaki K, Ohnishi Y, Shima T, Tanaka T, Ito K, Umezu M (2005) Development of an inexpensive first-aid type ventricular assist device driven by IABP consoles. In Proceedings of the 12th International conference on Biomedical Engineering, Singapore

Umezu M, Ye C-X, Nugent AH, Chang VP (1991) Advantages of the spiral vortex design in pneumatic blood pumps as demonstrated by dye-washout tests. Artificial Organs 14(4): 31-33

Yagi T, Yang W, Umezu M (2005) Stereoscopic PIV measurements on 3D swirling convergent flows inside a Spiral Vortex ventricular assist device. In Proceedings PIV'05, 6th International Symposium on Particle Image Velocimetry, Pasadena, CA, U.S.A.